PCP
PLANT & CELL PHYSIOLOGY

Light and Low-CO_2-Dependent LCIB–LCIC Complex Localization in the Chloroplast Supports the Carbon-Concentrating Mechanism in *Chlamydomonas reinhardtii*

Takashi Yamano[1,4], Tomoki Tsujikawa[1], Kyoko Hatano[2], Shin-ichiro Ozawa[3,5], Yuichiro Takahashi[3] and Hideya Fukuzawa[1,*]

[1]Graduate School of Biostudies, Kyoto University, Kyoto, 606-8502 Japan
[2]Graduate School of Human and Environmental Studies, Kyoto University, Kyoto, 606-8501 Japan
[3]Graduate School of Natural Science and Technology, Okayama University, Okayama, 700-8530 Japan
[4]Present address: Graduate School of Medicine, University of Tokyo, Tokyo, 113-0033 Japan
[5]Present address: Centre national de la recherché scientifique, UMR 7141, Institut de Biologie Physico-Chimique, 13 Rue Pierre et Marie Curie, 75005 Paris, France
*Corresponding author: E-mail, fukuzawa@lif.kyoto-u.ac.jp; Fax, +81-75-753–6127
(Received June 5, 2010; Accepted July 15, 2010)

The carbon-concentrating mechanism (CCM) is essential to support photosynthesis under CO_2-limiting conditions in aquatic photosynthetic organisms, including the green alga *Chlamydomonas reinhardtii*. The CCM is assumed to be comprised of inorganic carbon transport systems that, in conjunction with carbonic anhydrases, maintain high levels of CO_2 around ribulose-1, 5-bisphosphate carboxylase/oxygenase in a specific compartment called the pyrenoid. A set of transcripts up-regulated during the induction of the CCM was identified previously and designated as low-CO_2 (LC)-inducible genes. Although the functional importance of one of these LC-inducible genes, *LciB*, has been shown recently, the biochemical properties and detailed subcellular localization of its product LCIB remain to be elucidated. Here, using yeast two-hybrid, immunoprecipitation and mass spectrometry analyses we provide evidence to demonstrate that LCIB interacts with the LCIB homologous protein LCIC in yeast and in vivo. We also show that LCIB and LCIC are co-localized in the vicinity of the pyrenoid under LC conditions in the light, forming a hexamer complex of approximately 350 kDa, as estimated by gel filtration chromatography. LCIB localization around the pyrenoid was dependent on light illumination and LC conditions during active operation of the CCM. In contrast, in the dark or under high-CO_2 conditions when the CCM was inactive, LCIB immediately diffused away from the pyrenoid. Based on these observations, we discuss possible functions of the LCIB–LCIC complex in the CCM.

Keywords: Carbon-concentrating mechanism • *Chlamydomonas reinhardtii* • Chloroplast • *LciB* • Photosynthesis • Pyrenoid.

Abbreviations: AD, activation domain; AR, *Hsp70A-RbcS2*; BD, DNA-binding domain; BSA, bovine serum albumin; CA, carbonic anhydrase; CCM, carbon-concentrating mechanism; CDS, coding sequence; Ci, inorganic carbon; DTT, dithiothreitol; EST, expressed sequence tag; GFP, green fluorescent protein; HC, high-CO_2; LC, low-CO_2; LCE, light-dependent CO_2 gas exchange; OD, optical density; PBS, phosphate-buffered saline; RNAi, RNA interference; Rubisco, ribulose-1,5-bisphosphate carboxylase/oxygenase; VLC, very low-CO_2; WT, wild type.

Introduction

In nature, the ambient carbon dioxide (CO_2) concentration of 0.038% [low-CO_2 (LC)] is one of the major limiting factors for photosynthesis. To adapt to LC environments, aquatic photosynthetic organisms have developed a carbon-concentrating mechanism (CCM) to optimize their photosynthetic rate. Although aquatic photosynthesis under LC conditions shows characteristics similar to those seen in C_4 photosynthesis, the microalgal CCM and C_4 photosynthetic mechanisms are very different. The CCM, uptake systems for dissolved inorganic carbon (Ci; CO_2 and bicarbonate) increases the CO_2 concentration at the site of ribulose-1, 5-bisphosphate carboxylase/oxygenase (Rubisco) (Badger et al. 1980, Fukuzawa et al. 2001, Giordano et al. 2005, Spalding 2008). So far, at least five types of transport systems involved in Ci uptake have been characterized in cyanobacteria, including three bicarbonate transporters and two CO_2 uptake systems (Price et al. 2008). However, very little is known about eukaryotic photosynthetic organisms.

In eukaryotes, the unicellular green alga *Chlamydomonas reinhardtii* has served as a model system to study the CCM (Badger et al. 1980, Moroney and Ynalvez 2007, Spalding 2008). Although a number of LC-inducible genes required for acclimation to LC conditions have been cloned and characterized using cDNA subtraction and cDNA array techniques (Burow et al. 1996, Miura et al. 2004, Yamano et al. 2008, Yamano and

Plant Cell Physiol. 51(9): 1453–1468 (2010) doi:10.1093/pcp/pcq105, available online at www.pcp.oxfordjournals.org

Fukuzawa 2009), only high-light activated 3 (HLA3), a putative ABC-type transporter (Im and Grossman 2002), has been linked definitively to the CCM (Duanmu et al. 2009a).

In eukaryotic algae, Rubisco is mainly located in the pyrenoid, a prominent and electron-dense subcellular structure in the chloroplast stroma. In *Chlamydomonas*, approximately 90% of Rubisco is present in the pyrenoid when the CCM is active (Kuchitsu et al. 1991, Rawat et al. 1996, Morita et al. 1997). So far, several models of the CCM in *Chlamydomonas* have been proposed based on the structure of the pyrenoid (Moroney and Ynalvez 2007, Spalding 2008). First, Ci outside of the cells is acquired and delivered to the chloroplast stroma by putative HCO_3^- and/or CO_2 transporters on both the plasma membrane and the chloroplast envelope. Secondly, HCO_3^- is transported into the thylakoid lumen by unidentified HCO_3^- transporters, followed by conversion of HCO_3^- to CO_2 by the catalytic activity of an α-type carbonic anhydrase (CAH3) located in the acidic thylakoid lumen, which generates CO_2 at >10-fold higher levels than the concentration of HCO_3^- (Raven 1997, Karlsson et al. 1998, Hanson et al. 2003, Mitra et al. 2005). In many algae, including *Chlamydomonas*, pyrenoid tubules are parts of the thylakoid membranes that penetrate into the pyrenoid matrix (Ohad et al. 1967). Based on these structures, it is proposed that CO_2 generated in the thylakoid lumen may diffuse through the pyrenoid tubules to the pyrenoid matrix where Rubisco fixes the CO_2, although this model has not been validated experimentally. Furthermore, CAH6, a β-type CA located in the chloroplast stroma, might be responsible for supplying CO_2 to Rubisco by recapturing CO_2 leaking from the pyrenoid matrix and helping to maintain a high concentration of Ci in the stroma (Mitra et al. 2004). To date, no *Chlamydomonas* mutants with a disrupted pyrenoid structure have been isolated, and the actual function of the pyrenoid in the CCM is still debated. However, because the pyrenoid and pyrenoid tubules are thought to play important roles in the CCM (Moroney and Ynalvez 2007), identifying proteins localized in the vicinity of the pyrenoid may lead to a better understanding of the CCM.

The *Chlamydomonas* genome sequence has helped to identify genes encoding candidate Ci transporters based on a number of criteria, including subcellular localization, similarity to other known transporters and expression that is regulated by CO_2 availability (Merchant et al. 2007). Several genes, including *Ccp1*, *Ccp2*, *LciA*, *LciB*, *Hla3*, *Lci1* and *Rh1*, have been identified as candidates with roles in Ci transport (Burow et al. 1996, Chen et al. 1997, Im and Grossman 2002, Miura et al. 2004, Soupene et al. 2002, Soupene et al. 2004, Wang and Spalding 2006, Yamano et al. 2008). Among these genes, *LciB* was recently characterized as a Ci transport-related gene. *LciB*, firstly identified as an LC-inducible gene (Miura et al. 2004), was regulated during CCM induction through CCM1/CIA5, a zinc-binding regulatory factor (Kohinata et al. 2008). Molecular analyses of the high-CO_2 requiring *pmp1* and *ad1* mutants, which cannot grow in LC conditions but can grow either in high-CO_2 (5% CO_2, HC) or very low-CO_2 (0.005% CO_2, VLC) conditions, revealed that the corresponding Pmp1/Ad1 protein is encoded by *LciB* (Wang and Spalding 2006). This unusual and conspicuous phenotype provides evidence that multiple Ci transport systems operate in *Chlamydomonas* and that they are differentially regulated based on the available CO_2 concentration (Vance and Spalding 2005, Wang and Spalding 2006, Duanmu et al. 2009a). Furthermore, it was first observed that the immunofluorescence signal of LCIB was concentrated mainly in a discreet region surrounding the pyrenoid (Duanmu et al. 2009b). However, although the functional importance of *LciB* under LC conditions has been shown, its biochemical properties and detailed subcellular localization in response to CO_2 concentrations remain to be elucidated.

In this study, we provide evidence that LCIB interacts with LCIC, a protein homolog of LCIB, in yeast and in vivo, and forms a high molecular weight complex under LC conditions. Furthermore, we show that the localization of the LCIB in the vicinity of the pyrenoid is closely dependent on light illumination and LC conditions, which correspond to the active state of the CCM. Based on these biochemical properties and subcellular localization, we discuss the functional importance of the LCIB–LCIC complex in the operation of CCM.

Results

Expression profiles of the LCIB and LCIC proteins

The expression of *LciB* and *LciC* during LC acclimation was reported previously at the mRNA level (Miura et al. 2004, Wang and Spalding 2006, Yamano et al. 2008). To evaluate the expression of the respective gene products in the photosynthetically wild-type (WT) 5D strain, which was used throughout this study, crude protein extracts were prepared from 5D cells grown under HC and LC conditions, electrophoresed and then probed with antibodies against LCIB or LCIC synthetic polypeptides (ANAPTMESPEPVHP and PTMDSPELANMN, respectively) (**Fig. 1A**). The apparent molecular sizes of the protein bands detected were approximately 48 and 49 kDa, respectively. The LCIB and LCIC mature polypeptides were slightly accumulated under HC conditions, and their protein levels were induced after shifting to LC conditions, reaching saturation within 6 h.

LCIB and LCIC levels in 5D cells were compared with those in the previously isolated HC-requiring C16 and *pmp1* mutants (**Fig. 1B**). In the *Ccm1* mutant C16 cells (Fukuzawa et al. 1998, Fukuzawa et al. 2001), the LCIB and LCIC protein levels were slightly induced under LC conditions but significantly reduced compared with those of the WT. In *pmp1*, LCIB was not detected because of a nonsense mutation in the *LciB* sequence (Wang and Spalding 2006). Unexpectedly, in addition to the absence of LCIB, the protein level of LCIC was significantly reduced in *pmp1*.

Isolation and characterization of LciB RNAi strains

Previously, *LciB* was shown to be essential for cell growth and efficient photosynthesis under LC conditions, but not under

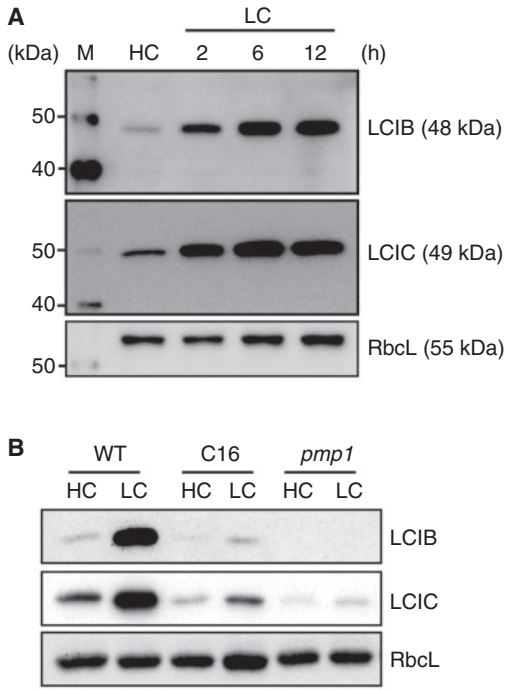

Fig. 1 Expression profiles of LCIB and LCIC proteins. (A) Crude protein extracts were prepared from wild-type cells (WT) grown under high-CO_2 (HC) and low-CO_2 (LC) conditions, and used for Western blotting analyses with antibodies against LCIB, LCIC and RbcL. The times in hours after switching to LC conditions are indicated. RbcL was used as a loading control, and 40 and 50 kDa protein size markers are indicated. (B) The protein expression profiles of LCIB and LCIC in WT, C16 and *pmp1*. Crude protein extracts were prepared from HC-acclimated cells (HC) and cells grown under LC conditions for 6 h (LC).

HC and VLC conditions, by analyzing a deletion mutant *ad1* (Wang and Spalding 2006). To elucidate the functions of LCIB further, we examined the physiological phenotypes of a mutant of LCIB generated by RNA interference (RNAi). The accumulation of LCIB was significantly reduced in five of the 36 transformants, of which two RNAi strains, C2 and D5, were selected for analyses (**Supplementary Fig. S1**).

First, the growth of WT, C2 and D5 was monitored by spotting cell suspensions onto agar plates with high salt medium under various CO_2 concentrations (**Fig. 2A**). Under HC and VLC conditions, the growth of C2 and D5 was not significantly different from that of the WT. In contrast, under LC conditions, C2 and D5 showed slower growth rates than the WT but did not die, as shown previously (Wang and Spalding 2006).

Next, to evaluate the photosynthetic characteristics of the RNAi strains, the rates of photosynthetic O_2 evolution under changing external Ci concentration were measured with WT and D5 cells acclimated to HC and LC conditions (**Fig. 2B**). At 10–100 μM Ci, LC-acclimated WT and D5 showed typical photosynthetic responses for cells expressing the CCM; the WT showed maximal and D5 showed approximately 90% of maximal photosynthetic rates at 100 μM Ci. However, while WT cells retained photosynthetic activity between 100 μM and 1 mM Ci, the photosynthetic rates of LC-acclimated D5 cells were reduced to approximately 55% of the maximal rate at around 500 and 700 μM Ci, and the rates increased again at higher concentrations of Ci, reaching a maximum at 4.5 mM Ci. In contrast, there were no significant differences between HC-grown WT and D5. Similar results were also obtained in the case of C2. This photosynthetic response curve of *LciB* RNAi strains was different from that of *ad1* reported previously in that LC-acclimated *ad1* cells showed a typical HC-requiring photosynthetic response curve and the photosynthetic rate was only approximately 13% compared with that of the WT at 100 μM Ci (Wang and Spalding 2006). Therefore, we again measured the photosynthetic O_2 evolution of *pmp1* as well as *ad1-3* (a walled progeny of *ad1*). At 100 μM Ci, the photosynthetic rate of LC-acclimated *ad1-3* and *pmp1* showed maximal and 70% of maximal photosynthetic rates, respectively. However, the photosynthetic rates of *ad1-3* and *pmp1* were reduced to approximately 50 and 45% of the maximal rate at 700 and 500 μM Ci, respectively, and the rates increased again at higher concentrations of Ci, reaching a maximum at 4.5 mM Ci. There were no significant differences among HC-acclimated *ad1-3*, *pmp1* and WT. These results indicated that the photosynthetic response curves of *ad1-3* and *pmp1* were similar to those of RNAi strains and showed multiphasic responses of photosynthesis to increasing Ci.

Finally, to evaluate further CO_2-dependent photosynthetic acclimation of the *LciB* RNAi strain, we measured the light-dependent CO_2 gas exchange (LCE) activities of HC- and LC-grown WT and D5 with a supply of air providing VLC and LC conditions (**Fig. 2C**). When the cells were grown under VLC conditions in a chamber for 10 min with illumination at 2,000 μmol photons $m^{-2}\,s^{-1}$, LC-grown WT and D5 exhibited LCE activities of 93.1 and 68.5 μmol CO_2 $mgChl^{-1}\,h^{-1}$, respectively, approximately 5.2 and 4.3 times higher than those of HC-grown WT and D5 values of 18.0 and 15.9 μmol CO_2 $mg\,Chl^{-1}\,h^{-1}$, respectively. When grown under LC conditions in the chamber, WT exhibited approximately 3.4 times higher LCE activity in LC compared with HC conditions (120.1 compared with 35.2 μmol CO_2 $mgChl^{-1}\,h^{-1}$). In contrast, D5 had approximately only 1.2 times higher LCE activity in LC compared with HC conditions (45.3 compared with 37.1 μmol CO_2 $mgChl^{-1}\,h^{-1}$). These results indicated that the LCE of LC-grown D5 increased when grown under VLC conditions, and that the LCE was significantly reduced under LC conditions.

Subcellular localization of LCIB and LCIC

Both LCIB and LCIC were predicted to be soluble proteins because of the lack of any transmembrane domains, and both proteins were indeed detected in the soluble protein fraction (**Supplementary Fig. S2**). To examine LCIB localization, we constructed a transgenic *Chlamydomonas* line harboring *Chlamydomonas*-adapted green fluorescent protein (GFP) fused to LCIB driven by the constitutive *Hsp70A-RbcS2* (AR) promoter and observed the GFP fluorescence signal under LC

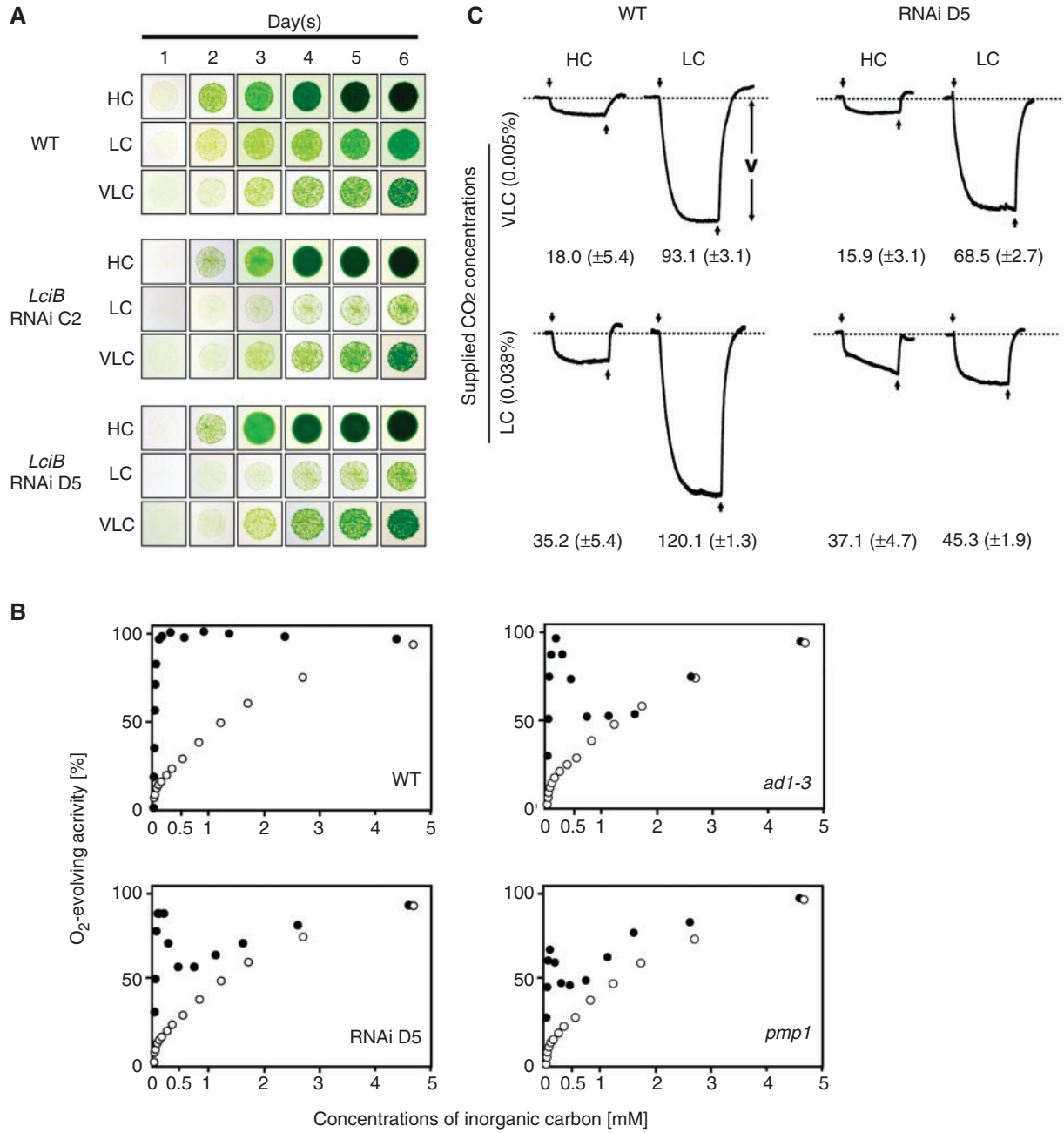

Fig. 2 Physiological phenotypes of *LciB* RNAi cells. (A) Spot tests for growth of WT and *LciB* RNAi cells. Cells were grown in closed chambers supplied with 5% CO_2 (HC), ambient air (LC) or 0.005% CO_2 (VLC) for 6 d. (B) Typical responses of net O_2-evolving activities to external dissolved Ci of WT, *LciB* RNAi cells, *ad1-3* and *pmp1*. Cells were grown under HC conditions or acclimated to LC conditions for 12 h. Open and filled circles represent O_2-evolving activities of the HC- or LC-grown cells, respectively. (C) Light-dependent CO_2 gas exchange profiles over time for WT and *LciB* RNAi cells. Cells were grown under HC conditions or acclimated to LC conditions for 12 h, and suspended in fresh HS medium to a concentration of 5 μg Chl ml^{-1}. Standard N_2 gas containing VLC or LC was supplied to the cell chamber. Cells were exposed to actinic light for 10 min, and the rate of CO_2 gas exchange activity (v) was measured from light on (downward-facing arrow) until light off (upward-facing arrow). The numbers given under the kinetics represent the light-dependent CO_2 gas exchange activities (μmol CO_2 mg Chl^{-1} h^{-1}) obtained from at least three independent experiments, which are shown as means ± SD.

and VLC conditions (**Fig. 3A**). The GFP signal was not clearly detected in any specific subcellular compartments in the cells grown under HC for 24 h. On the other hand, under LC and VLC conditions, GFP signals from the transgenic line (LCIB–GFP) were detected as a ring-like structure around the pyrenoid, as shown in a previous report (Duanmu et al. 2009b). To verify the localization further, we carried out indirect immunofluorescence assays on LC-grown cells using antibodies against LCIC

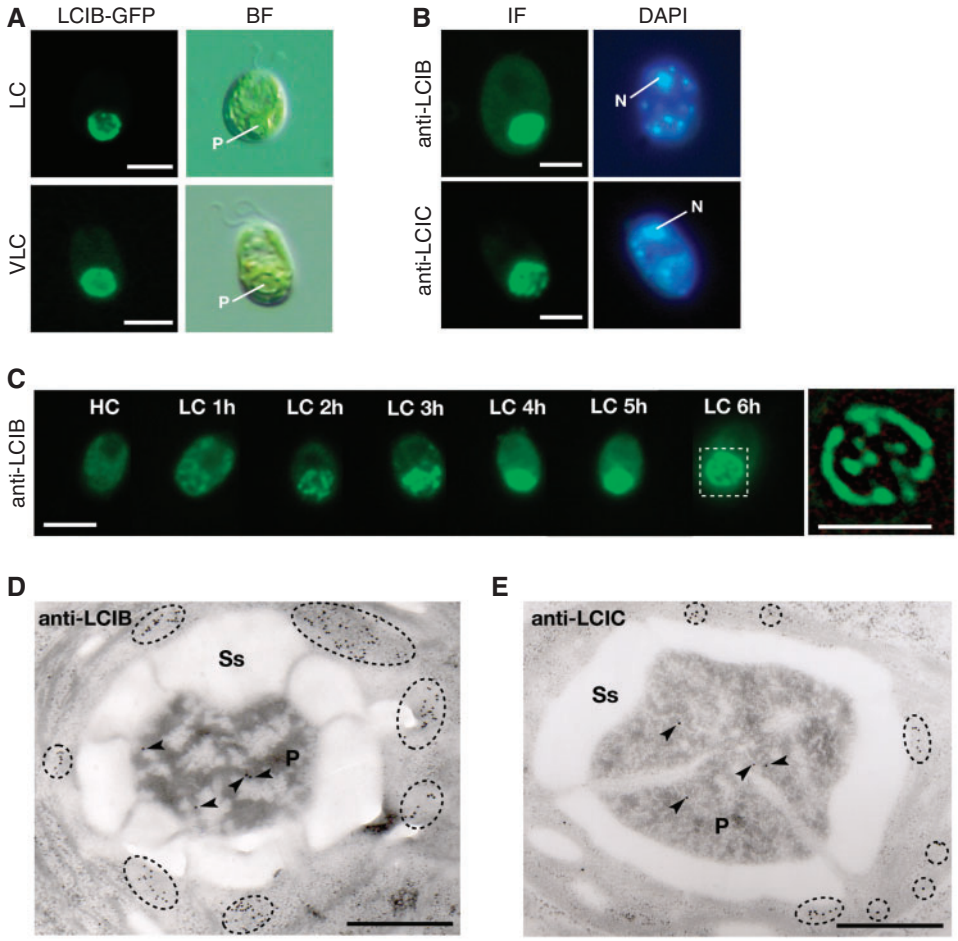

Fig. 3 Subcellular localization of LCIB and LCIC. (A) Fluorescent signals of the LC- or VLC-grown cells harboring GFP-tagged LCIB driven by the *Hsp70A-RbcS2* (AR) promoter (Schroda et al. 2000). BF, bright field image. P, pyrenoid. Bars = 5 µm. (B) Indirect immunofluorescence (IF) assay showing antibody labeling of LCIB and LCIC, and DAPI (4′,6-diamidino-2-phenylindole) labeling of the nucleus (N) in cells grown under LC conditions for 12 h. Bars = 5 µm. (C) Indirect immunofluorescence assay of LCIB localization during CCM induction. Cells grown under HC conditions were shifted to LC conditions, and the immunofluorescence signals over time were observed until 6 h. The area outlined in the image at LC 6 h is magnified in the right-hand column. Bars = 5 µm. (D and E) Immunoelectron micrographs with purified anti-LCIB or anti-LCIC antibodies. Cells were grown under LC conditions for 6 h. Magnified images at the region of a pyrenoid (P) are shown. Gold particles around the pyrenoid and those in the pyrenoid matrix are shown by dotted circles and by arrowheads, respectively. Ss, starch sheaths. Bars = 1 µm.

as well as LCIB. In addition to a ring-like structure around the pyrenoid, fluorescent signals corresponding to LCIB and LCIC were also detected in the pyrenoid (**Fig. 3B**). Next, to examine whether LCIB localization changed with altered levels of supplied CO_2, LCIB localization was traced using an indirect immunofluorescence assay during the CCM induction process (**Fig. 3C**). Under HC conditions, the immunofluorescent signal was dispersed around the entire region of the chloroplast as a cup-shaped structure. After shifting to LC conditions, the immunofluorescent signal aggregated in the vicinity of the pyrenoid to form ring-like and tubule-like structures (**Fig. 3C**, right-hand column). Because some thylakoids penetrate the pyrenoid, which are termed pyrenoid tubules (Ohad et al. 1967), LCIB in the pyrenoid may be localized along the pyrenoid tubules. A three-dimensional view of immunofluorescent signals corresponding to LCIB localization is shown in **Supplementary Movie 1** online.

To analyze further the localization of LCIB and LCIC under LC conditions, we carried out immunogold electron microscopic analyses (**Fig. 3D, E**, and full images shown in **Supplementary Fig. S4, S5**). Thin sections of *Chlamydomonas* cells were probed with affinity-purified LCIB or LCIC antibodies and observed using transmission electron microscopy. Immunogold densities in different cells are summarized in **Table 1**. It was shown that the respective immunogold labeling for LCIB and LCIC was 8.6- and 6.4-fold more abundant in the area around the pyrenoid compared with other areas of the stroma. Interestingly, immunogold signals around the starch sheaths were detected in clusters. These observations suggested that LCIB and LCIC are present close to each other, possibly forming

Table 1 Intracellular localization of LCIB and LCIC

	No. of immunogold particles μm^{-2}						
	Outside	**Cytoplasm**	**Nucleus**	**Stroma**	**Around pyrenoid**	**Pyrenoid matrix**	**Starch sheaths**
LCIB	0.65±0.84	1.58±0.47	2.01±0.88	1.77±0.79	15.20±2.65	2.70±1.86	0.45±0.74
LCIC	0.21±0.67	1.23±0.35	1.14±0.58	2.03±0.81	13.04±4.21	2.06±0.93	0.94±0.87

Immunogold densities in sections of different cells were calculated by dividing the number of immunogold particles by the area of the respective subcellular compartments. The average densities±SD were calculated using five different cell sections. The area 'around pyrenoid' was defined as the area 350 nm outside of the starch sheaths in the chloroplast. The stroma area includes the thylakoid area and was calculated by subtracting the area of 'around pyrenoid' + 'pyrenoid matrix' + 'starch sheaths' from the total area of the chloroplast. The cytoplasmic area was calculated by subtracting the total area of the chloroplast and the nucleus from the cell area. The area (μm^2) was calculated using ImageJ software.

a complex in vivo in the vicinity of the pyrenoid under LC conditions.

Light- and low-CO_2-dependent LCIB localization

As shown in **Fig. 3C**, LCIB immunofluorescent signals detected throughout the chloroplast under HC conditions accumulated in the vicinity of the pyrenoid after transfer to LC conditions, suggesting that LCIB localization in the vicinity of the pyrenoid could be important for operation of the CCM. To determine whether the subcellular compartmentalization of LCIB was affected by light and CO_2, as in the case of induction of the CCM, the fluorescent signals of GFP-fused LCIB were traced in different environmental conditions of light illumination and CO_2 concentrations (**Fig. 4**). First, transgenic cells harboring GFP-fused LCIB were grown under LC conditions in light (**Fig. 4A**, LC-light) and then transferred to dark conditions for 2 h under LC conditions (**Fig. 4A**, LC-dark). Initially, under LC-light conditions, GFP signals were observed as a ring-like structure in the vicinity of the pyrenoid. However, within 1 h after transfer to LC-dark conditions, the signals diffused from the pyrenoid throughout the entire chloroplast and aggregated into punctuate structures. Next, cells grown under LC-light conditions were transferred to HC conditions in the light (**Fig. 4B**, HC-light). The GFP signals also diffused from the pyrenoid throughout the chloroplast within 20 min, and this diffusion was not affected by the addition of 10 μM DCMU, which inhibits photosynthetic electron flow and CCM operation (Badger et al. 1980). Finally, to determine whether the change in subcellular compartmentalization was reversible or not, cells grown under HC-light conditions for 1 h when GFP signals had diffused throughout the chloroplast were once again transferred to LC-light conditions, and then the cells were observed after 5 min, 20 min, 1 h and 2 h (**Fig. 4C**). The fluorescent signals re-accumulated in the vicinity of the pyrenoid within 1 h, and this aggregation of signals was not observed in the presence of DCMU under LC-light conditions. When HC-grown cells were placed in LC-dark conditions, relocation of signals to the pyrenoid was not observed. Using western blotting analyses, it was observed that the amount of LCIB was not altered by switching CO_2 or light conditions within 1 h (**Supplementary Fig. S3**). These observations indicated that subcellular localization of LCIB depended on light as well as CO_2-limiting stress.

LCIB interacts with LCIC and forms a high molecular weight complex

The similar localization of LCIB and LCIC in the vicinity of the pyrenoid under LC conditions suggested a potential biochemical interaction between LCIB and LCIC. To evaluate the protein–protein interaction, yeast two-hybrid assays were carried out (**Fig. 5**). cDNA fragments covering the entire coding sequences of *LciB* and *LciC* were fused to the activation domain (AD) and DNA-binding domain (BD) coding sequences. The resulting plasmid combinations of AD and BD (LCIB-AD and LCIB-BD, LCIB-AD and LCIC-BD, LCIC-AD and LCIB-BD, and LCIC-AD and LCIC-BD) were co-transformed into yeast cells, and the growth of yeast transformants was monitored in selective SD medium. Yeast cells harboring every combination of plasmids could grow, indicating that LCIB interacts with LCIC and that LCIB and LCIC interact with themselves. Yeast cells harboring only LCIB- or LCIC-fused BD could not survive in selective media, suggesting that LCIB or LCIC alone did not have transcriptional activation potential.

To assess the in vivo interaction between LCIB and LCIC, immunoprecipitation assays were carried out. Because the anti-LCIB and anti-LCIC antibodies were not suitable for immunoprecipitation assays, we constructed transgenic *Chlamydomonas* cells harboring FLAG-tagged LCIB. The C-terminal end of LCIB was tagged by fusing the *LciB* coding region to three copies of a sequence encoding the FLAG (DYKDDDDK) sequence (Hernan et al. 2000), and then the FLAG-tagged *LciB* was transformed into the WT. Transformants containing the epitope tag were screened using an anti-LCIB antibody (**Supplementary Fig. S6**), and the 2F8 transgenic line expressing FLAG-tagged LCIB (LCIB-FLAG) was used for further pull-down assays. Soluble proteins were extracted from LC-acclimated WT and 2F8 cells and immunopurified using anti-FLAG affinity gel. To detect the components that specifically interacted with LCIB, FLAG affinity-purified samples were subjected to Western blotting analyses (**Fig. 6A**). The fact that both antibodies against FLAG polypeptide and LCIB cross-reacted with the 51 kDa protein band in the immunoprecipitate of 2F8 indicated that the LCIB-FLAG fusion protein was 51 kDa in size, and the 48 kDa protein band was endogenous LCIB. In addition, using an antibody against LCIC, a 49 kDa band was shown to include the endogenous LCIC. These results strongly suggested that

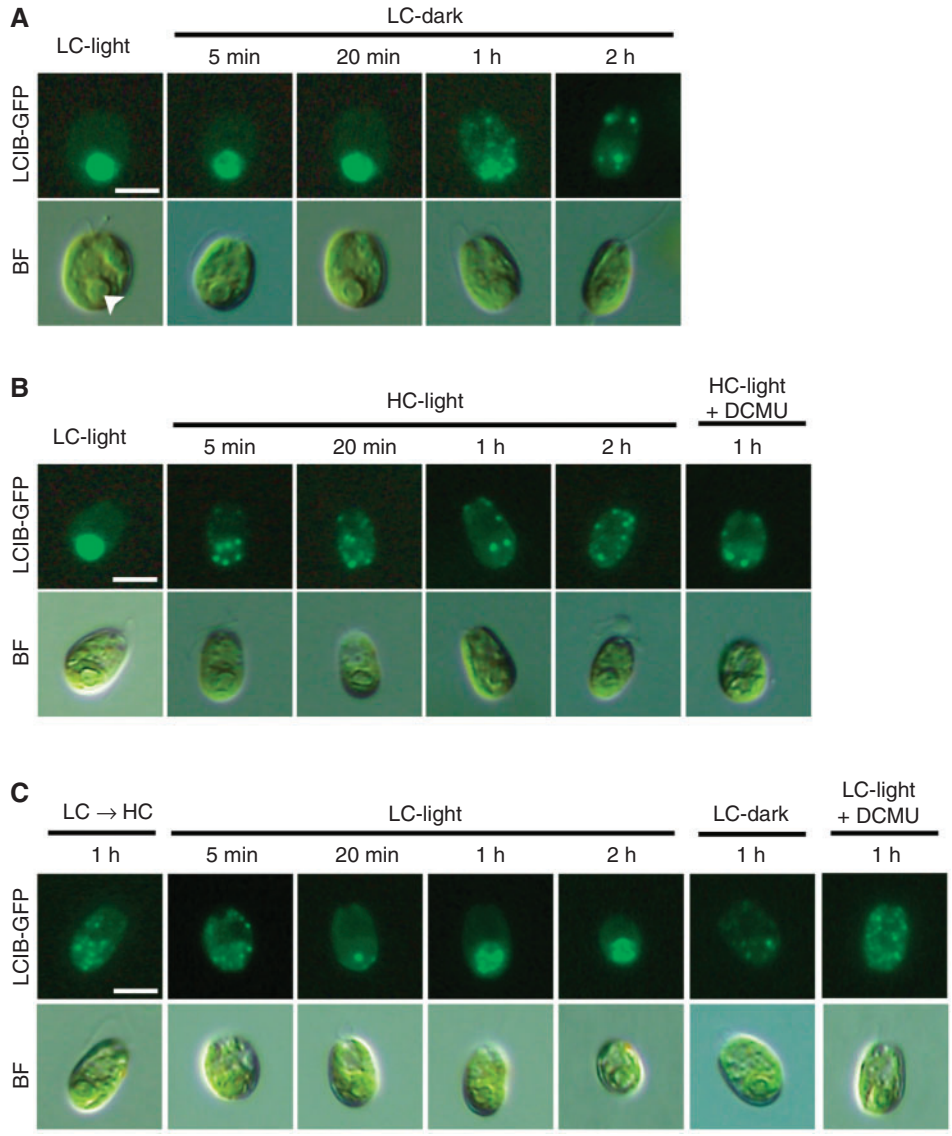

Fig. 4 Light- and low-CO_2 dependent LCIB localization in the vicinity of the pyrenoid. (A) LCIB localization after switching from light to dark. Cells harboring GFP-fused LCIB were acclimated to the LC conditions in the light (LC-light), following a shift to LC conditions in the dark (LC-dark), and GFP signals were observed for 2 h. An arrowhead indicates the pyrenoid. BF, bright field image. Bar = 5 μm. (B) LCIB localization after switching from LC to HC conditions. Cells acclimated to LC-light conditions were washed, transferred to HC-bubbled HS medium and grown under HC conditions in light (HC-light). DCMU (10 μM) was added to the HC-bubbled HS medium (+ DCMU). Bar = 5 μm. (C) LCIB localization after switching from HC to LC conditions. Cells grown in LC-light conditions were transferred to HC-light conditions as described above and cultured for 1 h. Then, the cells were again washed, transferred to fresh HS medium and cultured under LC-light or LC-dark conditions. DCMU was added to the fresh HS medium (+ DCMU). Bar = 5 μm.

LCIB interacted with LCIB as well as LCIC in vivo under LC conditions. To examine the potential interaction of CCM-related proteins with the LCIB–LCIC complex, Western blotting analyses were performed using antibodies against LCI5, an LC-inducible phosphoprotein (Turkina et al. 2006), and CAH3. However, neither of the two antibodies cross-reacted with immunoprecipitates derived from 2F8. Next, to determine whether LCIB and LCIC were associated with the thylakoid membrane, total solubilized protein and thylakoid membrane fractions were separated by SDS–PAGE and subjected to Western blotting analyses using antibodies against CAH3, LCIB, LCIC, RbcL and D1 protein in PSII (**Fig. 6B**). As reported previously, D1 and CAH3 were detected in the thylakoid membrane fraction, while RbcL was not present in this fraction. Both LCIB and LCIC were detected in the total protein fraction but not in the thylakoid membrane fraction, as was the case for RbcL. These results indicated that LCIB and LCIC were mainly located in stroma as soluble proteins.

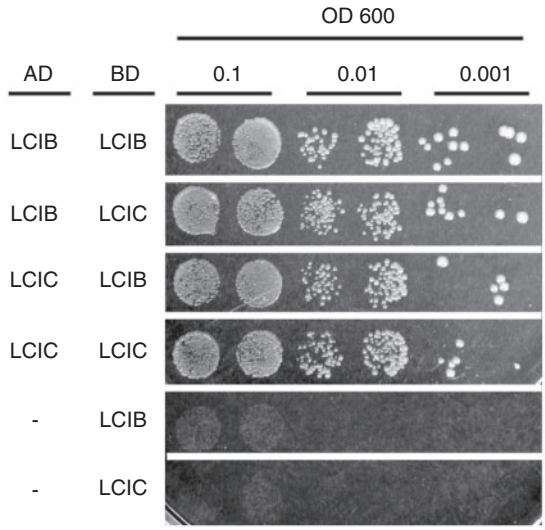

Fig. 5 Interaction of LCIB and LCIC in yeast cells. The colonies represent dilution series of each strain grown on selective SD medium (−His, −Leu, −Trp). AD, the activation domain; BD, the DNA-binding domain.

Considering the fact that LCIB and LCIC interacted with each other in vivo, it is possible that LCIB and LCIC could form a complex in vivo. To verify this possibility, we estimated the molecular mass of the complex in non-denaturing conditions. In soluble protein fractions extracted from HC- or LC-grown WT cells, WT cells treated with HC for 1 h (LC to HC 1h) and FLAG-tag immunoprecipitate (IP) from transgenic 2F8 cells grown under LC conditions were separated by size exclusion chromatography into fractions, and then subjected to Western blotting analyses using LCIB and LCIC antibodies (**Fig. 6C**). In HC-grown cells, a relatively small amount of LCIB was detected mainly in fraction 48, corresponding to a molecular mass of 150 kDa, and also detected, in part, in fraction 40, corresponding to a molecular mass of 350 kDa (**Supplementary Fig. S7**). LCIC was also detected mainly in the same fractions corresponding to 150 and 350 kDa, respectively. In LC-grown cells, LCIB was mainly detected at both 150 and 350 kDa, but the main portion of LCIC was detected at 350 kDa. Although the molecular masses of monomeric LCIB and LCIC were approximately 50 kDa each in denaturing conditions (**Fig. 1A**), LCIB and LCIC were present as an approximately 350 kDa complex under LC conditions. Although LCIB in LC-acclimated cells diffused away from the pyrenoid after switching to HC conditions for 1 h (**Fig. 4B**), the 350 kDa LCIB–LCIC complex seemed to remain. Furthermore, the affinity-purified immunoprecipitate indicated that the intact 350 kDa LCIB–LCIC complex persisted.

In order to determine the components of the complex, two independent mass spectrometric analyses were performed. First, immunoprecipitates from LC-grown cells were separated by SDS–PAGE and then stained using the Flamingo fluorescence dye (**Fig. 6D**). Two bands were detected in 2F8, but not

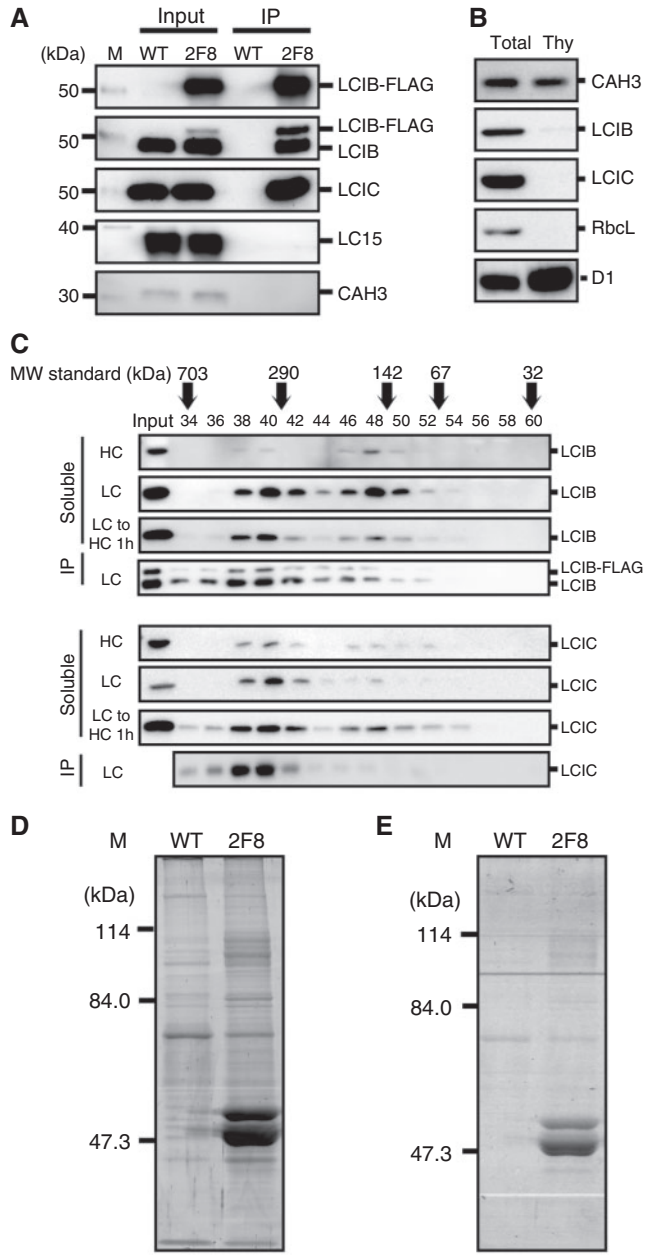

Fig. 6 Interaction of LCIB and LCIC in vivo. (A) The soluble protein fractions (Input) and immunoprecipitates (IP) from the WT and the transgenic cells harboring FLAG-tagged LCIB (2F8) were probed by antibodies against FLAG, LCIB, LCIC, LCI5 and CAH3. The top panel indicates the chemiluminescence image obtained using an anti-FLAG antibody. (B) Total cell proteins (Total) and the thylakoid membrane fraction (Thy) were probed with antibodies against CAH3, LCIB, LCIC, RbcL and D1. (C) Estimation of the molecular masses of LCIB and LCIC in vivo. Fraction numbers (34–60), which refer to fractions from the size exclusion column, are indicated above each lane. As molecular weight (MW) standards, fractions corresponding to the molecular size markers, thyroglobulin (703 kDa), glutamate dehydrogenase (290 kDa), lactate dehydrogenase (142 kDa), enolase (67 kDa) and myokinase (32 kDa) are indicated by arrows with the respective molecular mass. (D and E) FLAG-affinity purified proteins extracted from the WT and the transformant 2F8 were separated by SDS–PAGE and stained using Flamingo (D) and ProQ Diamond (E).

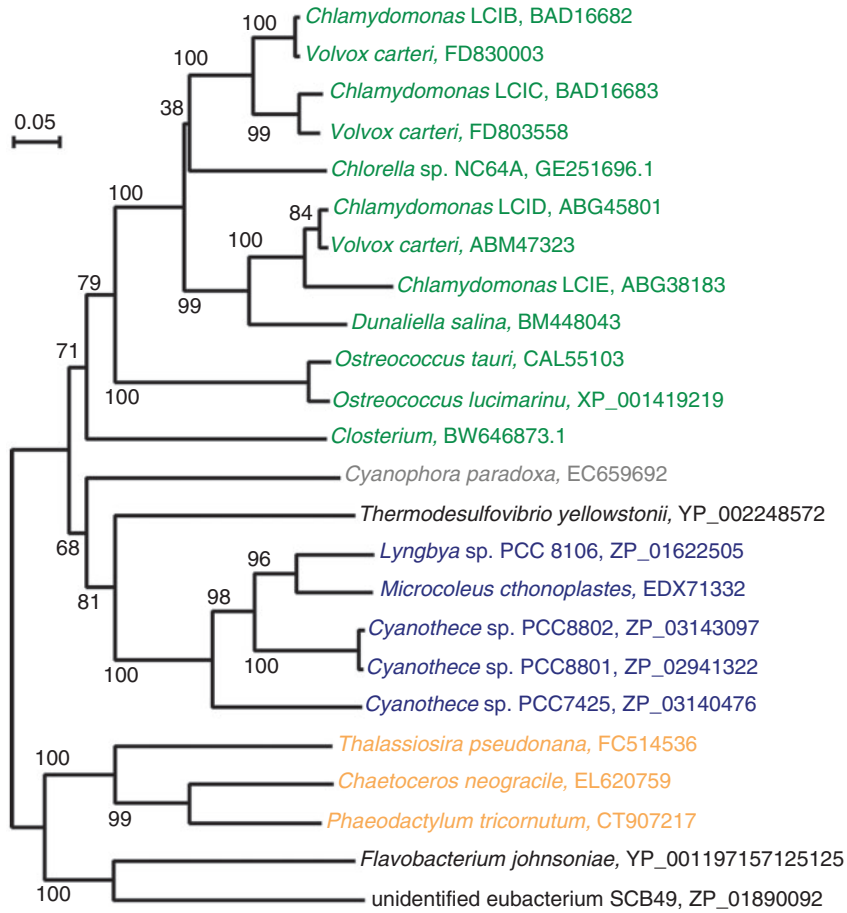

Fig. 7 Phylogenetic tree of LCIB homologs. The phylogenetic tree was constructed using the Neighbor–Joining method with 1,000 bootstrap replications. Bootstrap percentages are shown at the branch points of the dendrogram. GenBank accession numbers are given after the species names. Green, gray, blue, yellow and black represent green algae, Glaucophyta, cyanobacteria, diatoms and bacteria, respectively.

in the WT, at approximately 48 and 51 kDa. Tryptic digests of these two bands were analyzed by liquid chromatography–tandem mass spectrometry (LC-MS/MS), revealing that the 48 and 51 kDa bands contained polypeptides from both LCIB and LCIC, and that there were no other components (**Supplementary Table S1**). Staining the same gel with ProQ-Diamond suggested that the 51 kDa band of FLAG-tagged LCIB and the 48 kDa band of LCIB and/or LCIC were phosphorylated (**Fig. 6E**). Next, in order to analyze the entire set of polypeptides in the immunoprecipitate from cells grown under LC or HC conditions for 1 h after a shift from LC conditions, in-solution digestion and LC-MS/MS were performed. Although the quantity of polypeptide detected was significantly greater compared with in-gel digestion, there were no other components besides LCIB and LCIC (**Supplementary Table S2**).

Phylogenetic analysis of LCIB homologs

To date, the existence of LCIB homologous proteins has only been described in green algae such as *Chlamydomonas* (Miura et al. 2004) and *Ostreococcus* (Spalding 2008). To identify LCIB orthologs in other organisms, the full-length sequence of the LCIB protein was used in a tblastn search against expressed sequence tag (EST) databases in GenBank and genomic databases in JGI. Several organisms possessing LCIB counterparts were identified, including green algae (*Volvox carteri*, *Dunaliella salina*, *Chlorella* sp. NC64A and *Closterium*), Glaucophyta (*Cyanophora paradoxa*), diatoms (*Phaeodactylum tricornutum*, *Thalassiosira pseudonana* and *Chaetoceros neogracile*), cyanobacteria (*Lyngbya* sp. PCC 8106, *Microcoleus cthonoplastes* and *Cyanothese*) and bacteria (*Thermodesulfovibrio yellowstonii*, *Flavobacterium johnsoniae* and unidentified eubacterium SCB49). Because the identification of LCIB orthologs was based on at least two amplifications of ESTs, several deduced amino acid sequences were partial, but small portions of the amino acid sequences were conserved in all organisms mentioned above and could be aligned using CLUSTAL X (Thompson et al. 1997; **Supplementary Fig. S8**). From the multiple alignments, a phylogenetic tree of LCIB orthologs was constructed using the Neighbor–Joining method on 1,000 bootstrap replications using the PHYLIP phylogeny inference package (**Fig. 7**).

The LCIB orthologs were conserved in representative aquatic photosynthetic organisms known to have a CCM, but no LCIB orthologs could be identified in land plants.

Discussion

Properties of LCIB and LCIC proteins

In this study, we have shown that LCIB and LCIC protein levels were strongly induced under LC conditions (**Fig. 1A**). Although both LCIB and LCIC are assumed to have chloroplast-targeting signals at their N-terminal ends and the predicted molecular sizes of the respective mature polypeptides are 42.8 and 43.7 kDa, Western blotting analyses estimated the apparent molecular sizes of mature LCIB and LCIC to be approximately 48 and 49 kDa, respectively. Therefore, it is possible that the processing sites of the premature polypeptides may be different from the predicted sites or that some unknown post-translational modification of LCIB and LCIC occurred in the cells. Different sizes of bands and different levels of protein accumulation in HC-acclimated cells were detected using anti-LCIB and anti-LCIC antibodies, strongly suggesting that each antibody detected a specific single band corresponding to LCIB and LCIC, respectively. In the Western blotting analyses in **Fig. 1B**, the accumulation of LCIB was lost in *pmp1* because of a nonsense mutation in the *LciB* coding sequence of *pmp1* (Wang and Spalding 2006). Interestingly, the levels of LCIC were also significantly reduced in *pmp1*. Furthermore, although an *LciB* RNAi strain showed normal expression of *LciC* at the mRNA level, the accumulation of LCIC protein was much lower than that of the WT (**Supplementary Fig. S1**). Considering that LCIB and LCIC interact in vivo and form a protein complex, LCIC could become unstable when LCIB is not accumulated in the cell.

Formation of an LCIB–LCIC complex

From the results of gel filtration analysis, both LCIB and LCIC were mostly eluted in the same fraction corresponding to a molecular mass of approximately 350 kDa, indicating that the two proteins formed a complex with a molecular mass of around 350 kDa. In addition, yeast two-hybrid assays showed that both LCIB and LCIC interacted with each other and with themselves. Furthermore, LCIB and LCIC were immunoprecipitated using a transformant expressing FLAG-tagged LCIB, indicating that these two proteins existed as a complex in vivo. When the LCIB complex was purified from the immunoprecipitate and subjected to Western blotting analysis using the anti-LCIB antibody, two bands, which were equivalent to LCIB-FLAG and internal LCIB, respectively, were detected. This suggested that the LCIB complex included more than one LCIB. To determine the components of the complex, we performed mass spectrometric analysis on the immunoprecipitated proteins. Only peptides corresponding to LCIB and LCIC were detected using mass spectrometric analysis. Therefore, it is likely that the 350 kDa protein complex was comprised of just these two proteins.

Subcellular localization of the LCIB–LCIC complex

Based on the predicted localization of LCIB by the ChloroP program (Emanuelsson et al. 1999) and lack of any predicted transmembrane regions in LCIB, it was proposed that LCIB is localized to the stroma of the chloroplast (Miura et al. 2004, Grossman et al. 2007, Spalding 2008). In this study, we elucidated the subcellular localization of LCIB and LCIC by constructing transgenic cells harboring GFP-tagged LCIB, using an indirect immunofluorescent assay, and by immunogold labeling. The fluorescence signals of LCIB and LCIC were detected as tubule-like structures in the pyrenoid as well as a ring-like structure around the pyrenoid. Although LCIB is not functional under VLC conditions (Wang and Spalding 2006), the localization of LCIB under VLC conditions was not significantly different from that under LC conditions.

We further investigated changes in LCIB localization in response to environmental changes in CO_2 and light. Under LC-light conditions, GFP signals were observed as a ring-like structure in the vicinity of the pyrenoid, but the signals diffused from the pyrenoid throughout the chloroplast under LC-dark or HC-light conditions. Interestingly, fluorescent signals of LCIB–GFP under LC-dark and HC-light conditions were detected as aggregated punctuate structures, suggesting that LCIB localization could change while in the complex. This observation was consistent with the finding that the 350 kDa LCIB–LCIC complex was not dissociated after shifting from LC to HC conditions. The fluorescence signal derived from LCIB–GFP just after shifting from LC to HC conditions was strengthened because of this aggregated form of the LCIB–LCIC complex. Conversely, in HC-acclimated cells, fluorescence signals derived from LCIB–GFP were not observed. In HC-acclimated cells, as shown by an indirect immunofluorescence assay, LCIB was localized to the entire region of chloroplast stroma, and not aggregated, suggesting that the fluorescent signals derived from LCIB–GFP were below the detection limit, although the amount of LCIB was not significantly altered by switching CO_2 or light conditions (**Supplementary Fig. S3**). Furthermore, LCIB re-accumulated in the vicinity of the pyrenoid within 1 h after shifting from HC to LC conditions. This change in localization did not occur under LC-dark or LC-light conditions in the presence of DCMU. Based on the above observations, and considering that the CCM is not active under dark conditions and that blocking photosynthetic electron transport markedly decreases the ability of cells to acclimate to changes in Ci (Badger et al. 1980), the localization of LCIB in the vicinity of the pyrenoid was clearly dependent on the active state of the CCM. It was reported previously that the immunofluorescence signal of LCIB was dispersed throughout the entire chloroplast stroma as well as around the pyrenoid under LC conditions (Duanmu et al. 2009b). Considering that LCIB could change its localization reversibly and quickly (**Fig. 3**), it is possible that the experimental conditions during the indirect immunofluorescent assay in the previous report could affect the localization of LCIB and the dispersed LCIB might correspond to that observed under LC-dark conditions in this study.

Distribution of LCIB homologs in aquatic photosynthetic organisms

A search of the available databases for land plants failed to find a sequence that aligned well with LCIB. Aquatic photosynthetic organisms possessing LCIB homologs also have a pyrenoid or carboxysome structures, except for *Cyanophora* and *Ostreococcus*. Pyrenoid-containing plant species are found within all major groups of algae, with the exception of the *Cyanophyta*, while the only terrestrial plant with a recognized pyrenoid is hornwort. However, *Cyanophora* also have pyrenoid-like structures called the central bodies in the cyanelle. Based on this evidence, it is possible that LCIB homologs have an ancient origin and its function is related to pyrenoid- or carboxysome-based carbon fixation in aquatic conditions. The function of LCIB homologs identified in some non-photosynthetic bacteria remains to be elucidated.

Biological function of the LCIB–LCIC complex

Even though the data presented here help identify the detailed subcellular localization and biochemical properties of the LCIB–LCIC complex, the actual function of the complex remains unknown. Because both LCIB and LCIC were localized in the vicinity of the pyrenoid, and starch sheaths developed around the pyrenoid and became thicker under LC conditions (**Supplementary Fig. S4, S5**) as shown previously (Kuchitsu et al. 1988, Ramazanov et al. 1994), it is possible that the function of the LCIB–LCIC complex could be related to the developing pyrenoid structure and/or formation of starch sheaths. However, the pyrenoid or the accumulation of Rubisco in the pyrenoid are not always essential for the CCM, as in the case of the pyrenoid-lacking alga *Chloromonas* (Morita et al. 1998). Although starch sheaths cover the pyrenoid under LC conditions (Kuchitsu et al. 1988, Ramazanov et al. 1994), starch-less *Chlorella* and *Chlamydomonas* mutants were able to induce a fully active CCM, indicating that starch sheath formation itself is not involved in the operation of the CCM in *Chlorella* and *Chlamydomonas* (Plumed et al. 1996, Villarejo et al. 1996). Furthermore, considering that *pmp1*, *ad1* and *LciB* RNAi strains developed a pyrenoid in the normal manner and formed starch sheaths around the pyrenoid under LC conditions (data not shown), and LCIB was not a starch-binding protein and could localize around the pyrenoid even in a starch-less mutant (**Supplementary Fig. S9**), it is unlikely that the LCIB–LCIC complex is associated with pyrenoid development and/or starch sheath formation.

Recent investigations have pointed out that *Chlamydomonas* possess at least three acclimation states in response to environmental CO_2 concentrations (Vance and Spalding 2005, Wang and Spalding 2006, Duanmu et al. 2009a), which were subsequently defined as the HC, LC and VLC states. The multiphasic response of photosynthesis in the *LciB* RNAi strain was consistent with these multiple acclimation states. Under VLC conditions, which correspond to approximately 10–100 μM Ci, LCIB is not essential for acclimation. The RNAi strain showed near maximal levels of photosynthetic activity and could acclimate to VLC conditions as in the case of WT cells. Under LC conditions, which correspond to approximately 100 μM to 1 mM Ci, LCIB is essential for growth. Therefore, cells defective in LCIB could not retain the CCM, and their photosynthetic activity decreased. In HC conditions, which correspond to >1 mM Ci, LCIB is not essential, and the photosynthetic activity again increased. This multiphasic response of photosynthesis to increasing Ci concentrations was supported by measuring LCE activity. The LCE activity of the RNAi strain decreased significantly when the cells were incubated in LC but not VLC conditions. Although, at this stage, we cannot fully explain the differences between our results and the previously reported *ad1* phenotype, they might be due to the different experimental conditions in measuring photosynthetic activity, e.g. the number of data points, pH conditions during the measurements (pH 7.8 in this study and pH 7.3 in Wang and Spalding 2006) and growth conditions.

The localization of LCIB in the vicinity of the pyrenoid under LC conditions suggested two functional possibilities. One is that LCIB localized in the vicinity of the pyrenoid plays some roles to trap CO_2 leaking from the pyrenoid matrix and to transfer the captured CO_2 to stromal carbonic anhydrase CAH6 (**Fig. 8A**), although the functional importance and regulation of CAH6 is not clear. A recent genetic screen of suppressor mutants of *ad1* also supported the hypothesis, in that LCIB functions downstream of CAH3 in the CCM and probably plays a barrier role by trapping CO_2 leaking from the pyrenoid matrix (Duanmu et al. 2009b). In this model, the CO_2 actually leaks into stroma, but CAH6 located around the pyrenoid may be responsible for supplying CO_2 for Rubisco by recapturing CO_2 leaking from the pyrenoid matrix (Mitra et al. 2004). Although CAH6 was not identified as one of the components of the LCIB–LCIC complex, it remains possible that LCIB–LCIC and CAH6 might cooperate to support CCM without direct interaction.

The other is that the LCIB–LCIC complex may function as a structural barrier to avoid the leakage of CO_2 and maintain CO_2 concentrations in the pyrenoid matrix for efficient CO_2 fixation (**Fig. 8B**). In contrast, in the *LciB* mutant, CO_2 may be able to leak easily from the pyrenoid matrix, and consequently photosynthetic activity decreases (**Fig. 8C**). Because CAH6 was not identified as one of the components of the LCIB–LCIC complex in this study, it is reasonable to suppose that CAH6 is not directly associated with the LCIB–LCIC complex. Therefore, there could be two possibile cases in those CAH6 may be present or degraded in the LCIB RNAi strain. When CAH6 could be detected in the LCIB RNAi strain showing decreased photosynthetic activities under LC conditions, it is possible that CAH6 is not important for CCM or it cannot trap CO_2 leaked from the pyrenoid in the absence of LCIB–LCIC complex. If the CAH6 could not be detected in the LCIB RNAi strain, the LCIB–LCIC complex could function to support CA activities in stroma by relatively loose molecular interaction. Evaluation of CAH6 accumulation in the LCIB RNAi strain could

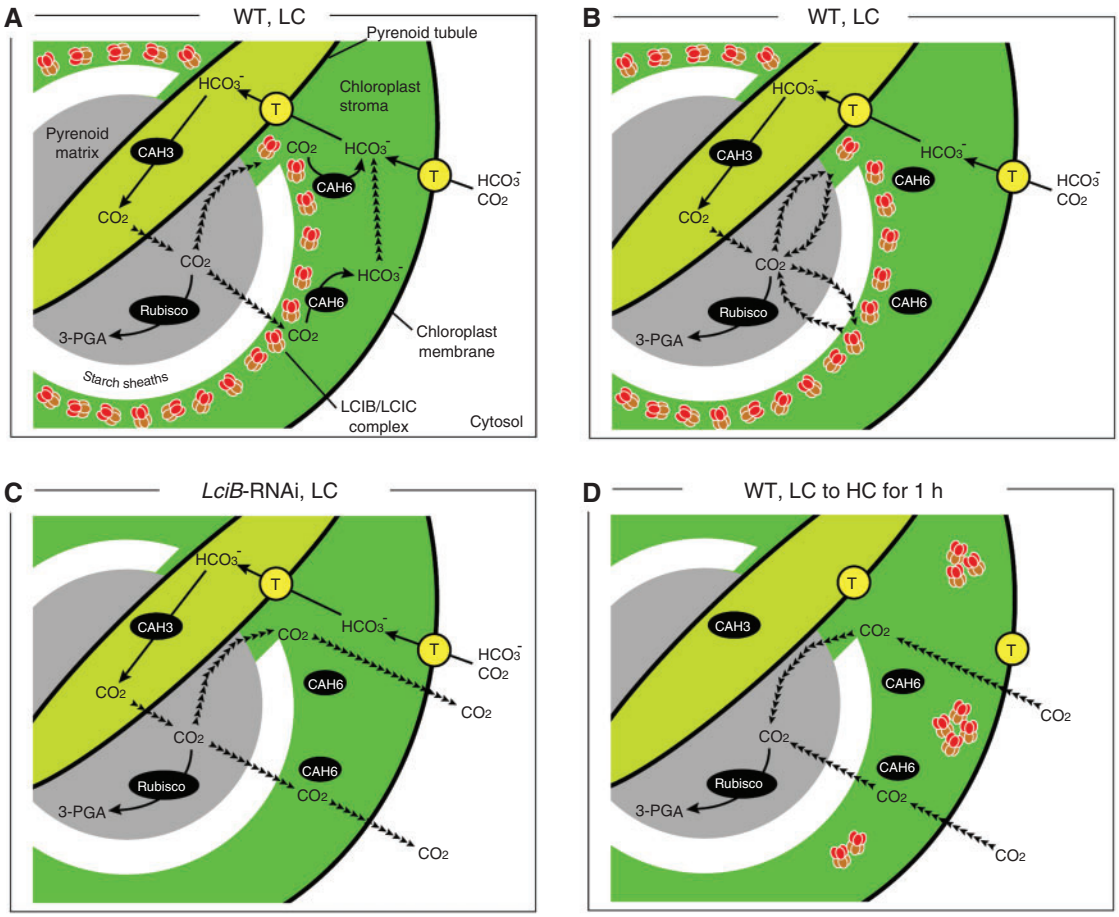

Fig. 8 Schematic diagram illustrating the roles of the LCIB–LCIC complex. (A) Functional model of the LCIB–LCIC complex in CO_2 recapturing and recycling functionally associated with CAH6, as described previously (Duanmu et al. 2009b). This model is based on the proposed *Chlamydomonas* CCM model (Moroney and Ynalvez 2007) and evidence that pyrenoid tubules penetrate into the pyrenoid matrix, as shown in Ohad et al. (1967) and **Supplementary Fig. S4** and **S5**. Because CAH6 is reported to be differentially concentrated around starch sheaths (Mitra et al. 2004), it is assumed that concentrated HCO_3^- around the starch sheaths is transported by a potential HCO_3^- transporter located in the thylakoid membranes near the starch sheaths. The potential HCO_3^- transporters located in the chloroplast and thylakoid membranes are indicated by a circled 'T'. The potential CO_2 transporters and/or channels operating under LC conditions are also indicated by a circled 'T' because it is possible that CO_2 transported into the chloroplast stroma is converted to HCO_3^- under the weak alkaline pH conditions in the stroma. The diffusion of CO_2 or HCO_3^- is indicated by dotted arrowheads. The LCIB–LCIC complex is depicted as a hetero-hexamer estimated from its molecular size. (B) Functional model of LCIB–LCIC as a structural diffusion barrier to avoid the leakage of CO_2 and maintain CO_2 concentrations in the pyrenoid matrix under LC conditions. (C) Leakage of CO_2 from the pyrenoid matrix in *LciB* RNAi strains under LC conditions. (D) Passive entry of CO_2 into the pyrenoid matrix after a switch from LC to HC conditions for 1 h leads to diffusion of the LCIB–LCIC complex into the chloroplast stroma, possibly because there is no requirement for the complex around the pyrenoid.

reveal these possibilities. Also, generation of knockout mutants of CAH6 and examining their phenotypes under LC conditions could help us to understand its role in CCM.

Considering that the *LciB* mutant showed almost the same levels of photosynthetic activity as WT cells under VLC conditions, it is reasonable to suppose that Rubisco can fix the majority of the CO_2 transported into the pyrenoid matrix by different acclimation systems from the LCIB–LCIC system, which normally operates under LC conditions.

No components other than LCIB and LCIC could be identified in the LCIB–LCIC complex using mass spectrometric analyses, suggesting that the possible structural barrier consisted of only LCIB and LCIC. Likewise, in cyanobacteria, CcmK1-4 and CcmL with no functional motifs were crystallized into a hexamer and a pentamer, respectively, with a central, charged pore surrounding the carboxysome where Rubisco was located (Kerfeld et al. 2005, Tanaka et al. 2008). Based on this structure, CcmK1-4 and CcmL are thought to create a specialized barrier that may regulate the flow of metabolites into and out of the carboxysome. Furthermore, it is possible that the LCIB–LCIC complex located in the vicinity of the pyrenoid interferes with the passive entry of CO_2 into the pyrenoid matrix under the switch from LC to HC conditions; this could be why LCIB diffuses rapidly away from the pyrenoid and throughout the

chloroplast by shifting from LC to HC conditions (**Fig. 8D**). Because the LCIB–LCIC complex was successfully affinity purified from *Chlamydomonas* cells, the three-dimensional structure of the LCIB–LCIC complex could be determined by cryo-electron microscopy and single particle analysis (Frank 2002), leading to a better understanding of the function of the LCIB–LCIC complex in the CCM.

Materials and Methods

Cells and growth conditions

The *C. reinhardtii* 'Dangeard' strain 5D (*nit1-305*, *cw15*, *mt*$^-$) used as a photosynthetically WT strain was provided by Dr. Peter Lefebvre (Tam et al. 1995). A high-CO_2-requiring mutant, C16 (*ccm1*), was described previously (Fukuzawa et al. 1998, Fukuzawa et al. 2001). Another high-CO_2-requiring mutant, *pmp1*, was provided by Dr. Martin Spalding (Spalding et al. 1983). Cells were cultured in TAP medium (Harris 1989) for maintenance. For photosynthetic growth, cells were cultured in buffered HS medium supplemented with 20 mM MOPS (pH 7.2) and grown at 28°C under continuous illumination using white fluorescent lamps (120 µmol photons m^{-2} s^{-1}), with bubbling of ordinary air containing 0.038% CO_2 (low-CO_2, LC) or air enriched with 5% CO_2 (high-CO_2, HC). VLC conditions were obtained by mixing LC with compressed, CO_2-free air. For experiments in which cells were shifted from HC to LC conditions, cells were harvested by centrifugation at 600×*g* for 5 min at 28°C and transferred to fresh HS medium. Throughout the experiments, the cell densities of the cultures were kept at $<3\times10^7$ cells ml^{-1}, corresponding to an optical density (OD) of 0.4 at 730 nm to avoid shading effects on the cells.

Spot tests for growth were performed by suspending actively growing cells in HS medium to an OD of 0.15 at 730 nm, spotting 15 µl of each cell suspension onto agar HS plates, and then the plates were kept in growth chambers in HC, LC or VLC conditions for 6 d.

Measurement of photosynthetic activity and light-dependent CO_2 gas exchange activity

The affinity of cells for Ci was evaluated by measuring the rate of dissolved Ci-dependent photosynthetic O_2 evolution. *Chlamydomonas* cells grown under HC or LC conditions were harvested by centrifugation at 600×*g* for 5 min and then resuspended in 50 mM HEPES buffer (pH 7.8) at 20 µg of Chl ml^{-1}. Photosynthetic oxygen evolution was measured using a Clark-type oxygen electrode (Hansatech Instruments) as reported previously (Yamano et al. 2008).

The cells were harvested after stress treatments and resuspended in fresh HS medium at 5 µg of Chl ml^{-1}. CO_2 exchange activity of the cell suspension was measured at 28°C using an open infrared gas analysis system that records the rate of CO_2 exchange as a function of time, as reported previously (Yamano et al. 2008).

Western blotting analyses

Detailed methods for the preparation of crude protein extract, soluble and insoluble protein fractions, and thylakoid membranes are described in the **Supplementary Methods** online. For the detection of target proteins, crude protein extracts from freshly harvested cells were resuspended in an equal volume of 2× SDS gel loading buffer [100 mM Tris–HCl, pH 6.8, 200 mM dithiothreitol (DTT), 4% SDS, 0.2% bromophenol blue, 20% glycerol] and heated to 65°C for 10 min. Typically, 10 µg of crude protein extract was separated by 10% (w/v) acrylamide SDS–PAGE. After electrophoresis, proteins were electrophoretically transferred to polyvinylidene difluoride (PVDF) membranes (Bio-Rad) at 300 mA for 1 h. Membranes were blocked with 5% (w/v) non-fat skim milk (Wako) in phosphate-buffered saline (PBS) for 1 h at room temperature. Blocked membranes were washed for 5 min with PBS containing 0.1% (v/v) Tween-20 (PBS-T) and inoculated with the following antibodies in PBS-T for 1 h at room temperature: rabbit anti-LCIB antibody (1:5,000 dilution); rabbit anti-LCIC antibody (1:10,000 dilution); rabbit anti-CAH1 antibody (1:2,500 dilution); rabbit anti-CAH3 antibody (1:2,500 dilution); rabbit anti-RbcL antibody (1:10,000 dilution); rabbit anti-D1 antibody (1:20,000 dilution); or mouse anti-FLAG M2 monoclonal antibody (1:20,000 dilution; Sigma). Membranes were rinsed once and washed with PBS-T three times for 5 min each. A horseradish peroxidase-conjugated goat anti-rabbit IgG antibody (1:5,000 dilution for LCIB, LCIC, CAH1 and CAH3; 1:20,000 dilution for RbcL and D1; GE Healthcare) or goat anti-mouse IgG antibody (1:20,000 dilution; GE Healthcare) were used as secondary antibodies for 1 h at room temperature. Membranes were washed as above, and immunologically positive signals were visualized by an enhanced chemiluminescence system in accordance with the manufacturer's instructions (GE Healthcare). Anti-LCIB and anti-LCIC antibodies were produced as described in the **Supplementary Methods** online.

Gel filtration chromatography

Protein crude extract prepared with P-buffer was centrifuged at 100,000×*g* for 1 h at 4°C and the resulting supernatants were filtrated through a 0.2 µm syringe filter (Pall). This soluble protein was subjected to gel filtration chromatography using an AKTA FPLC workstation with a Superdex 200 10/300 GL column (GE Healthcare) at 4°C. The elution was performed with P-buffer. The flow rate was 0.5 ml min^{-1} and the fraction volume was 0.25 ml. As molecular weight standards, the elution volumes of thyroglobulin (703 kDa), ferritin (438 kDa), glutamate dehydrogenase (290 kDa), aldolase (177 kDa) and lactate dehydrogenase (142 kDa) were used to estimate the apparent molecular mass.

Indirect immunofluorescence assay

Chlamydomonas cells were harvested by centrifugation and resuspended in PBS-T, and then affixed to poly-L-lysine-treated glass slides (Poly-Prep Slides, Sigma), by air-drying at room

temperature for 5 min. Cells were fixed with 4% (w/v) formaldehyde in PBS at room temperature for 20 min, treated with 100% ice-cold methanol at −30°C for 20 min, and then rehydrated by three 5 min washes in PBS at room temperature. The following procedures were all performed at room temperature. Cells were blocked with 5% (w/v) bovine serum albumin (BSA) in PBS for 1 h. The slides with fixed cells were incubated for 1 h with the anti-LCIB or anti-LCIC antibody diluted at 1:50 and 1:100, respectively, and then washed with PBS-T six times for 5 min each. Next, the cells were incubated for 1 h with the Alexa Fluor 488 goat anti-rabbit IgG (Invitrogen) diluted at 1:500, and washed as above. A series of digital optical sections of the fixed samples were obtained using an Axiophot fluorescence microscope (Zeiss) with a specific filter set (exciter D450–480, dichroic 425DCLP and emitter D510–560) (Chroma Technology Corp.). Fluorescence images were captured using a cooled charge-coupled device VB-7010 camera (KEYENCE).

Fluorescence microscopic analysis of GFP-tagged LCIB

Vector construction based on *Chlamydomonas*-adapted GFP (CrGFP) was carried out essentially as described previously (Fuhrmann et al. 1999). To generate a C-terminal fusion of GFP to LCIB, the entire genomic sequence of the *LciB* genes was amplified by PCR using Pyrobest DNA Polymerase (TAKARA BIO INC.) and fused in-frame with CrGFP. Transformed cells were selected by plating cell suspensions after electroporation onto TAP solid medium containing 10 μg ml^{-1} zeocin (Invitrogen) and observed using a Axioscope2 fluorescence microscope (Zeiss) with a GFP filter set (exciter D395/40, dichroic 425DCLP, and emitter D510/40) (Chroma Technology Corp.). Fluorescence images were captured using a cooled charge-coupled device VB-7010 camera (KEYENCE). For three-dimensional structural analyses of GFP fluorescence signals in transgenic *Chlamydomonas* cells, an LSM710 confocal laser-scanning microscope (Zeiss) was used with a ZEN LE image-processing program (http://www.zeiss.co.jp/micro).

Immunogold electron microscopy

Cells were frozen in liquid propane as described previously (Chida and Ueda 1992). They were then transferred to chilled acetone containing 1% (v/v) glutaraldehyde at −80°C. After 48 h at −80°C, samples were gradually warmed to −20°C. After rinsing with pure acetone and then with pure dimethylformamide at −20°C, the samples were embedded in LR White resin (London Resin Company). Blocks were polymerized under a UV lamp at −20°C for 24 h. Ultrathin sections were cut with a glass knife at 80 nm thicknesses on an ultramicrotome ULTRACUT N (Reichert-Nissei). For immunogold labeling, purified LCIB and LCIC antibodies were diluted at 12.5 and 20 μg ml^{-1}, respectively, in PBS containing 3% (w/v) BSA. Secondary antibody, AuroProbe EM-labeled rabbit IgG (H+L) conjugated to 10 nm gold particles (GE Healthcare), was diluted at 1:100 in PBS containing 3% (w/v) BSA. The immunogold-labeled sections were stained with 2% (w/v) uranyl acetate and lead citrate and were examined using an electron microscope (Hitachi H-7000).

Yeast two-hybrid assay

The yeast two-hybrid procedure was performed in accordance with the protocol for the HybriZAP-2.1 XR library construction kit (Stratagene). The *Eco*RI–*Xba*I fragments containing the full-length coding sequence (CDS) of *LciB* or *LciC* were subcloned into pAD-GAL4-2.1 (Stratagene) to make prey constructs. The *Eco*RI–*Eco*RI fragments containing the full-length CDS of *LciB* or *LciC* were subcloned into pBD-GAL4 Cam (Stratagene) to make bait constructs.

Immunoprecipitation

The constitutive *Hsp70A-RbcS2* (AR) promoter was used to express the FLAG-tagged LCIB. Three copies of the FLAG coding sequence (Castrucci et al. 1992) were inserted into the *LciB* coding sequence just before the stop codons. The FLAG-tagged *LciB* construct was used to transform WT cells by electroporation (Shimogawara et al. 1998). Transformants were selected on TAP agar plates containing 10 mg l^{-1} zeocin (Invitrogen) and screened by Western analysis using the anti-LCIB antibody or anti-FLAG M2 monoclonal antibody (Sigma). Soluble proteins extracted from WT and transgenic cells expressing the FLAG-tagged LCIB were immunoprecipitated with EZview Red ANTI-FLAG M2 Affinity Gel in accordance with the manufacturer's instructions (Sigma). Eluted proteins were separated by SDS–PAGE. The resulting gel was fixed and stained with Flamingo Fluorescent Gel Stain in accordance with the manufacturer's instructions (Bio-Rad), and an image was obtained using a FLA-3000 high-resolution scanner (Fuji Photo Film).

Identification of polypeptides by mass spectrometry

In-gel trypsin digestion of polypeptides was performed as described previously (Shevchenko et al. 1996) with some modifications for excised bands. We omitted reduction and alkylation steps, and extraction of the digested peptides was performed by centrifugation. In-solution digestion was performed using ProteasMAX surfactant (Promega) as described in the manufacturer's protocol and in a previous study (Wagner et al. 2008) with some modifications. FLAG-tagged LCIB complexes were solubilized with 0.2% (w/v) ProteasMAX surfactant, and subsequent reduction and alkylation steps were performed. The reduction step was in 5 mM DTT at 56°C for 20 min and the alkylation step was in 15 mM iodoacetamide at 25°C for 15 min in the dark, which were performed sequentially. We subsequently digested the proteins using trypsin (25 ng μl^{-1}) at 37°C for 3 h in the presence of 0.05% (w/v) ProteasMAX surfactant and the digestion process was stopped by adding 1% (v/v) trifluoroacetic acid and incubating at 25°C for 5 min. The resulting digests were purified by passing through a solid phase extraction tip (C-TIP; AMR), applied to a Paradigm MS4 dual solvent system (Michrom BioResources), and then mass spectra were measured using a Finnigan LTQ linear ion trap mass spectrometer (Thermo Fisher Scientific) (Ozawa et al. 2009).

Data analysis was performed using BioWorks software (version 3.3; Thermo Fisher Scientific) with three databases for *Chlamydomonas*: version 3.0 assembly in JGI, NC_005353 and NC_001638 in NCBI for nuclear, chloroplast and mitochondrial genome products, respectively. Criteria settings for data filtering were probability <0.001, Sf-final score >0.85 and number of top matches = 1.

Supplementary data

Supplementary data are available at PCP online.

Funding

This work was supported by the Ministry of Education, Culture, Sports, Science and Technology of Japan [Grants-in-Aid for Scientific Research Nos. 17018020 and 22380059 to H.F., and No. 18GS0318 to Y.T.]; the Japan Society for the Promotion of Science for Young Scientists [Research Fellowships (No. 05J01979 to T.Y. and No. 05J03605 to S.O.)].

Acknowledgments

We thank Dr. Shoko Fujiwara, Tokyo University of Pharmacy and Life Sciences for providing starch granules, and Mr. Hirobumi Nakano for technical assistance.

References

Badger, M., Kaplan, A. and Berry, J. (1980) Internal inorganic carbon pool of *Chlamydomonas reinhardtii*—evidence for a carbon-dioxide concentrating mechanism. *Plant Physiol.* 66: 407–413.

Burow, M., Chen, Z., Mouton, T. and Moroney, J. (1996) Isolation of cDNA clones of genes induced upon transfer of *Chlamydomonas reinhardtii* cells to low CO_2. *Plant Mol. Biol.* 31: 443–448.

Castrucci, M., Bilsel, P. and Kawaoka, Y. (1992) Attenuation of influenza A virus by insertion of a foreign epitope into the neuraminidase. *J. Virol.* 66: 4647–4653.

Chen, Z., Lavigne, L., Mason, C. and Moroney, J. (1997) Cloning and overexpression of two cDNAs encoding the low-CO_2-inducible chloroplast envelope protein LIP-36 from *Chlamydomonas reinhardtii*. *Plant Physiol.* 114: 265–273.

Chida, Y. and Ueda, K. (1992) Detection of actin on organelles of *Trebouxia potteri*, in particular on the surface of lysosomes. *Protoplasma* 171: 28–33.

Duanmu, D., Miller, A., Horken, K., Weeks, D. and Spalding, M. (2009a) Knockdown of limiting-CO_2-induced gene HLA3 decreases HCO_3^- transport and photosynthetic Ci affinity in *Chlamydomonas reinhardtii*. *Proc. Natl Acad. Sci. USA* 106: 5990–5995.

Duanmu, D., Wang, Y. and Spalding, M. (2009b) Thylakoid lumen carbonic anhydrase (CAH3) mutation suppresses air-dier phenotype of LCIB mutant in *Chlamydomonas reinhardtii*. *Plant Physiol.* 149: 929–937.

Emanuelsson, O., Nielsen, H. and Von Heijne, G. (1999) ChloroP, a neural network-based method for predicting chloroplast transit peptides and their cleavage sites. *Protein Sci.* 8: 978–984.

Frank, J. (2002) Single-particle imaging of macromolecules by cryo-electron microscopy. *Annu. Rev. Biophys. Biomol. Struct.* 31: 303–319.

Fuhrmann, M., Oertel, W. and Hegemann, P. (1999) A synthetic gene coding for the green fluorescent protein (GFP) is a versatile reporter in *Chlamydomonas reinhardtii*. *Plant J.* 19: 353–361.

Fukuzawa, H., Ishizaki, K., Miura, K., Matsueda, S., Ino-ue, T., Kucho, K., et al. (1998) Isolation and characterization of high-CO_2 requiring mutants from *Chlamydomonas reinhardtii* by gene tagging. *Can. J. Bot.* 76: 1092–1097.

Fukuzawa, H., Miura, K., Ishizaki, K., Kucho, K., Saito, T., Kohinata, T., et al. (2001) *Ccm1*, a regulatory gene controlling the induction of a carbon-concentrating mechanism in *Chlamydomonas reinhardtii* by sensing CO_2 availability. *Proc. Natl Acad. Sci. USA* 98: 5347–5352.

Giordano, M., Beardall, J. and Raven, J. (2005) CO_2 concentrating mechanisms in algae: mechanisms, environmental modulation, and evolution. *Annu. Rev. Plant Biol.* 56: 99–131.

Grossman, A., Croft, M., Gladyshev, V., Merchant, S., Posewitz, M., Prochnik, S., et al. (2007) Novel metabolism in *Chlamydomonas* through the lens of genomics. *Curr. Opin. Plant. Biol.* 10: 190–198.

Hanson, D., Franklin, L., Samuelsson, G. and Badger, M. (2003) The *Chlamydomonas reinhardtii cia3* mutant lacking a thylakoid lumen-localized carbonic anhydrase is limited by CO_2 supply to Rubisco and not photosystem II function in vivo. *Plant Physiol.* 132: 2267–2275.

Harris, E.H. (1989) The Chlamydomonas Sourcebook: A Comprehensive Guide to Biology and Laboratory Use. Academic Press, San Diego.

Hernan, R., Heuermann, K. and Brizzard, B. (2000) Multiple epitope tagging of expressed proteins for enhanced detection. *Biotechniques* 28: 789–793.

Im, C. and Grossman, A. (2002) Identification and regulation of high light-induced genes in *Chlamydomonas reinhardtii*. *Plant J.* 30: 301–313.

Karlsson, J., Clarke, A., Chen, Z., Hugghins, S., Park, Y., Husic, H., et al. (1998) A novel alpha-type carbonic anhydrase associated with the thylakoid membrane in *Chlamydomonas reinhardtii* is required for growth at ambient CO_2. *EMBO J.* 17: 1208–1216.

Kerfeld, C., Sawaya, M., Tanaka, S., Nguyen, C., Phillips, M., Beeby, M., et al. (2005) Protein structures forming the shell of primitive bacterial organelles. *Science* 309: 936–938.

Kohinata, T., Nishino, H. and Fukuzawa, H. (2008) Significance of zinc in a regulatory protein, CCM1, which regulates the carbon-concentrating mechanism in *Chlamydomonas reinhardtii*. *Plant Cell Physiol.* 49: 273–283.

Kuchitsu, K., Tsuzuki, M. and Miyachi, S. (1988) Changes of starch localization within the chloroplast induced by changes in CO_2 concentration during growth of *Chlamydomonas reinhardtii*-independent regulation of pyrenoid starch and stroma starch. *Plant Cell Physiol.* 29: 1269–1278.

Kuchitsu, K., Tsuzuki, M. and Miyachi, S. (1991) Polypeptide composition and enzyme activities of the pyrenoid and its regulation by CO_2 concentration in unicellular green algae. *Can. J. Bot.* 69: 1062–1069.

Lumbreras, V., Stevens, D. and Purton, S. (1998) Efficient foreign gene expression in *Chlamydomonas reinhardtii* mediated by an endogenous intron. *Plant J.* 14: 441–447.

Merchant, S., Prochnik, S., Vallon, O., Harris, E., Karpowicz, S., Witman G., et al. (2007) The *Chlamydomonas* genome reveals the evolution of key animal and plant functions. *Science* 318: 245–251.

Mitra, M., Lato, S., Ynalvez, R., Xiao, Y. and Moroney, J. (2004) Identification of a new chloroplast carbonic anhydrase in *Chlamydomonas reinhardtii*. *Plant Physiol.* 135: 173–182.

Mitra, M., Mason, C., Xiao, Y., Ynalvez, R., Lato, S. and Moroney, J. (2005) The carbonic anhydrase gene families of *Chlamydomonas reinhardtii*. *Can. J. Bot.* 83: 780–795.

Miura, K., Yamano, T., Yoshioka, S., Kohinata, T., Inoue, Y., Taniguchi, F., et al. (2004) Expression profiling-based identification of CO_2-responsive genes regulated by CCM1 controlling a carbon-concentrating mechanism in *Chlamydomonas reinhardtii*. *Plant Physiol.* 135: 1595–1607.

Morita, E., Abe, T., Tsuzuki, M., Fujiwara, S., Sato, N., Hirata, A., et al. (1998) Presence of the CO_2-concentrating mechanism in some species of the pyrenoid-less free-living algal genus *Chloromonas* (Volvocales, Chlorophyta). *Planta* 204: 269–276.

Morita, E., Kuroiwa, H., Kuroiwa, T. and Nozaki, H. (1997) High localization of ribulose-1,5-bisphosphate carboxylase/oxygenase in the pyrenoids of *Chlamydomonas reinhardtii* (Chlorophyta), as revealed by cryofixation and immunogold electron microscopy. *J. Phycol.* 33: 68–72.

Moroney, J. and Ynalvez, R. (2007) Proposed carbon dioxide concentrating mechanism in *Chlamydomonas reinhardtii*. *Eukaryot. Cell* 6: 1251–1259.

Ogawa, T., Miyano, A. and Inoue, Y. (1985) Photosystem-I-driven inorganic carbon transport in the cyanobacterium, *Anacystis nidulans*. *Biochim. Biophys. Acta* 808: 77–84.

Ohad, I., Siekevitz, P. and Palade, G. (1967) Biogenesis of chloroplast membranes. I. Plastid dedifferentiation in a dark-grown algal mutant (*Chlamydomonas reinhardtii*). *J. Cell Biol.* 35: 521–552.

Ozawa, S., Nield, J., Terao, A., Stauber, E.J., Hippler, M., Koike, H., et al. (2009) Biochemical and structural studies of the large Ycf4–photosystem I assembly complex of the green alga *Chlamydomonas reinhardtii*. *Plant Cell* 21: 2424–2442.

Plumed, M., Villarejo, A., de los Rios, A., GarciaReina, G. and Ramazanov, Z. (1996) The CO_2-concentrating mechanism in a starchless mutant of the green unicellular alga *Chlorella pyrenoidosa*. *Planta* 200: 28–31.

Price, G., Badger, M., Woodger, F. and Long, B. (2008) Advances in understanding the cyanobacterial CO_2-concentrating-mechanism (CCM): functional components, Ci transporters, diversity, genetic regulation and prospects for engineering into plants. *J. Exp. Bot.* 59: 1441–1461.

Ramazanov, Z., Rawat, M., Henk, M., Mason, C., Matthews, S. and Moroney, J. (1994) The induction of the CO_2-concentrating mechanism is correlated with the formation of the starch sheath around the pyrenoid of *Chlamydomonas reinhardtii*. *Planta* 195: 210–216.

Raven, J. (1997) CO_2-concentrating mechanisms: a direct role for thylakoid lumen acidification? *Plant Cell Environ.* 20: 147–154.

Rawat, M., Henk, M., Lavigne, L. and Moroney, J. (1996) *Chlamydomonas reinhardtii* mutants without ribulose-1,5-bisphosphate carboxylase-oxygenase lack a detectable pyrenoid. *Planta* 198: 263–270.

Schroda, M., Blöcker, D. and Beck, C. (2000) The HSP70A promoter as a tool for the improved expression of transgenes in *Chlamydomonas*. *Plant J.* 21: 121–131.

Shevchenko, A., Wilm, M., Vorm, O. and Mann, M. (1996) Mass spectrometric sequencing of proteins silver-stained polyacrylamide gels. *Anal. Chem.* 68: 850–858.

Shimogawara, K., Fujiwara, S., Grossman, A. and Usuda, H. (1998) High-efficiency transformation of *Chlamydomonas reinhardtii* by electroporation. *Genetics* 148: 1821–1828.

Soupene, E., Inwood, W. and Kustu, S. (2004) Lack of the Rhesus protein Rh1 impairs growth of the green alga *Chlamydomonas reinhardtii* at high CO_2. *Proc. Natl Acad. Sci. USA* 101: 7787–7792.

Soupene, E., King, N., Feild, E., Liu, P., Niyogi, K., Huang, C. and Kustu, S. (2002) Rhesus expression in a green alga is regulated by CO_2. *Proc. Natl Acad. Sci. USA* 99: 7769–7773.

Spalding, M. (2008) Microalgal carbon-dioxide-concentrating mechanisms: *Chlamydomonas* inorganic carbon transporters. *J. Exp. Bot.* 59: 1463–1473.

Spalding, M., Spreitzer, R. and Ogren, W. (1983) Reduced inorganic carbon transport in a CO_2-requiring mutant of *Chlamydomonas reinhardtii*. *Plant Physiol.* 73: 273–276.

Tam, L. and Lefebvre, P. (1995) Insertional mutagenesis and isolation of tagged genes in *Chlamydomonas*. *Methods Cell Biol.* 47: 519–523.

Tanaka, S., Kerfeld, C., Sawaya, M., Cai, F., Heinhorst, S., Cannon, G., et al. (2008) Atomic-level models of the bacterial carboxysome shell. *Science* 319: 1083–1086.

Thompson, J., Gibson, T., Plewniak, F., Jeanmougin, F. and Higgins, D. (1997) The CLUSTAL_X windows interface: flexible strategies for multiple sequence alignment aided by quality analysis tools. *Nucleic Acids Res.* 25: 4876–4882.

Turkina, M., Blanco-Rivero, A., Vainonen, J., Vener, A. and Villarejo, A. (2006) CO_2 limitation induces specific redox-dependent protein phosphorylation in *Chlamydomonas reinhardtii*. *Proteomics* 6: 2693–2704.

Vance, P. and Spalding, M. (2005) Growth, photosynthesis, and gene expression in *Chlamydomonas* over a range of CO_2 concentrations and CO_2/O_2 ratios: CO_2 regulates multiple acclimation states. *Can. J. Bot.* 83: 796–809.

Villarejo, A., Martinez, F., Plumed, M. and Ramazanov, Z. (1996) The induction of the CO_2 concentrating mechanism in a starch-less mutant of *Chlamydomonas reinhardtii*. *Physiol. Plant.* 98: 798–802.

Wagner, V., Ullmann, K., Mollwo, A., Kaminski, M., Mittag, M. and Kreimer, G. (2008) The phosphoproteome of a *Chlamydomonas reinhardtii* eyespot fraction includes key proteins of the light signaling pathway. *Plant Physiol.* 146: 772–788.

Wang, Y. and Spalding, M. (2006) An inorganic carbon transport system responsible for acclimation specific to air levels of CO_2 in *Chlamydomonas reinhardtii*. *Proc. Natl Acad. Sci. USA* 103: 10110–10115.

Yamano, T. and Fukuzawa, H. (2009) Carbon-concentrating mechanism in a green alga, *Chlamydomonas reinhardtii*, revealed by transcriptome analyses. *J. Basic Microbiol.* 49: 42–51.

Yamano, T., Miura, K. and Fukuzawa, H. (2008) Expression analysis of genes associated with the induction of the carbon-concentrating mechanism in *Chlamydomonas reinhardtii*. *Plant Physiol.* 147: 340–354.